RSC Advances

ROYAL SOCIETY OF CHEMISTRY

www.rsc.org/advances

Journal Name

ARTICLE

Luminescence properties of novel emission-tunable $NaSr_{(4-x-y)}Ba_x(BO_3)_3$: yEu^{2+} phosphor for white light emitting diodes

Received 00th January 20xx,
Accepted 00th January 20xx

DOI: 10.1039/x0xx00000x

www.rsc.org/

Jun Huang[a], Jian Dai[a], Degang Deng*[a], Hua Yu[b], Yinqun Li[a], Youjie Hua[a], Shilong Zhao[a], Chenxia Li[a], Shiqing Xu*[a]

Abstract: A serious of emission-tunable $NaSr_{(4-x-y)}Ba_x(BO_3)_3$: yEu^{2+} phosphors have been prepared by a conventional solid-state reaction method. The structure of $NaSr_{(4-x-y)}Ba_x(BO_3)_3$: yEu^{2+} have been investigated by Reitveld refinement of X-ray diffraction (XRD) patterns. The results indicated that the as-prepared samples showed the same crystals structure of $NaSr_4(BO_3)_3$ with cubic unit cell and space group of *Ia-3d*. With the increase of Ba^{2+} concentration, the Sr^{2+} sites were replaced by Ba^{2+} completely and the lattice parameter of unit cell increased from $a = b = c = 15.0710$ Å to 15.7266 Å. Both emission spectra and decay curves of $NaSr_{3.98}(BO_3)_3$: $0.02Eu^{2+}$ and $NaBa_{3.98}(BO_3)_3$: $0.02Eu^{2+}$ showed the existence of two different Eu^{2+} emission centers named Eu1 and Eu2. Eu2 was six-coordinated and Eu1 was eight-coordinated of oxygen. With the increase of Eu^{2+} concentration in $NaSr_{3-y}Ba(BO_3)_3$: yEu^{2+} sample, the emission intensity increased and reached the maximum at y=0.02. Then the concentration quenching phenomenon emerged due to the electric dipole-dipole interaction. Upon the cation substitutions (Sr^{2+} for Ba^{2+}) in the $NaSr_{(4-x-y)}Ba_x(BO_3)_3$: yEu^{2+} host, the emission peaks of Eu^{2+} blue-shifted from 609 nm to 544 nm and the thermal stability decreased, which was ascribed to the change of the covalency and the crystal field strength that the 5*d* orbital of the Eu^{2+} ion experiences. The CIE chromaticity coordinates of the obtained phosphors can be continuously tuned from orange-red (0.4795, 0.4070) to yellow-green (0.3432, 0.4665) by adjusting the Ba^{2+} concentration. The results demonstrate that the emission-tunable $NaSr_{(4-x-y)}Ba_x(BO_3)_3$: yEu^{2+} phosphor have a potential application for white light emitting diodes(w-LEDs).

1 Introduction

In the past several years, much more attention have been focused on the white light emitting diodes (w-LEDs) due to the advantages of high stability, energy saving capabilities and long working lifetime.[1-5] As a next generation lighting source, the w-LEDs have high promise to take place of the traditional fluorescent and incandescent lamp. Due to the strong absorption in the blue region and intense emission in the yellow region, the cerium-doped yttrium aluminum garnet (YAG: Ce^{3+}) phosphor was widely used in the w-LEDs. However, for the lacking of red emission, the w-LEDs packaged with YAG: Ce^{3+} phosphor exhibit poor color rendition and high color temperature. In order to obtain more selections for white LEDs, a new fabricated type of tunable emitting phosphors coupled with near ultraviolet (n-UV) chips has been developed. This combination method exhibited favorable properties, including excellent Color Rendition Index (CRI) values, tunable Commission Internationale de L'Eclairage (CIE) chromaticity coordinates and tunable Correlated Color Temperature (CCT).[9-13] Unfortunately, the emission tunable range of the phosphor with a single activated ion has been reported is limited to blue to yellow. Therefore, the development of color tunable phosphors from red to yellow is an important challenge.

The rare earth doped orthoborate phosphors which possess many advantages, such as significant absorption in the near ultraviolet (n-UV), good chemical stability, and relatively low sintering temperature, have been studied extensively.[14-19] As a novel orange-emitting borate phosphor, the $LiSr_{4-x}(BO_3)_3$: xEu^{2+} phosphor has been reported in the literature.[20, 21] However, the $NaSr_{4-x-y}Ba_x(BO_3)_3$: yEu^{2+} which shows the similar crystal structure with $LiSr_{4-x}(BO_3)_3$: xEu^{2+} was hardly researched. In this paper, a kind of emission-tunable (from orange-red to yellow-green) phosphor of $NaSr_{4-x-y}Ba_x(BO_3)_3$: yEu^{2+} has been studied systematically. The crystal structure and photoluminescence properties were studied deeply and the optimal composition was achieved for application in white LEDs.

2. Experimental

2.1 Sample preparation

The traditional high-temperature solid-state reaction method was used to synthesize the $NaSr_{(4-x-y)}Ba_x(BO_3)_3$: yEu^{2+} phosphor samples. The $SrCO_3$ (99.99%), $BaCO_3$ (99.99%), H_3BO_3 (99.99%), Na_2CO_3 (99.9%) and Eu_2O_3 (99.99%) were used as starting materials. Firstly, the stoichiometric amounts of the

[a] College of Materials Science and Engineering, China Jiliang University, Hangzhou 310018, China. Fax: +86-571-28889527; Tel: +86-571-86835781; E-mail: dengdegang@cjlu.edu.cn, sxucjlu@163.com .
[b] College of Materials and Environmental Engineering, Hangzhou Dianzi University, Hangzhou 310018, China.

staring materials were mixed in an agate mortar, then grinded thoroughly. Finally the mixture was sintered at 1000℃ with reductive atmosphere (95% N_2/5% H_2) for 4h in a high temperature tube furnace.

2.2 Characterization

The structures of all the synthesized samples were characterized by X-ray diffraction (XRD) using a Bruker Axs D2 PHASER Diffractometer, with Cu Ka radiation (λ = 1.5405 Å). The XRD data was collected between the 2θ range of 10 - 80° in the step scan mode with a measurement time of 1 s/step and a step size of 0.02° at room temperature. The emission and excitation spectra of the samples were collected by using a PL3-211-P Fluorescence Spectrometer (HORIBAJOBIN YVON, America) with an excitation source of a 450 W xenon lamp at room temperature. The diffuse reflectance spectra of the undoped samples were collected by a UV-3600 UV-Vis spectrometer (Shimadzu, Japan) and the reference material is $BaSO_4$ powder. Rietveld refinements on the XRD data were analyzed by the software of TOPAS.

2.3 White LED fabrication

White LED was fabricated by following steps. Firstly equably blend the LED packaging epoxy resin and $NaSr_{2.98}Ba(BO_3)_3$: $0.02Eu^{2+}$ phosphor. Secondly put the mixture into a substrate which can be used to control the shape and thickness of the film. Thirdly placed the substrate into an oven and baked at 60 ℃ for 4 h. Finally a luminescent thin film was obtained, and pasted the luminescent thin film up a 450 nm blue LED chip.

3 Results and discussion

3.1 Crystal structure

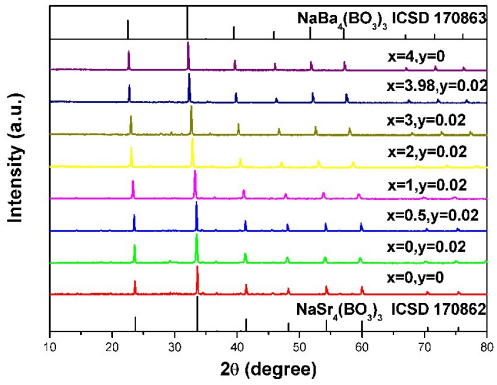

Figure 1 Powder X-ray diffraction patterns of $NaSr_{4-x-y}Ba_x(BO_3)_3$: yEu^{2+} with different x, y values

The XRD patterns of the $NaSr_{4-x-y}Ba_x(BO_3)_3$: yEu^{2+} with different x, y values were shown in Figure 1. The single phase of $NaSr_4(BO_3)_3$ (x = 0,y = 0) and $NaBa_4(BO_3)_3$ (x = 4,y = 0) were observed and all of the obtained diffraction peaks were matched well with the standard card of $NaSr_4(BO_3)_3$ (ICSD # 170862) and $NaBa_4(BO_3)_3$ (ICSD # 170863). With the increase of Ba^{2+} ions concentration, the positions of the diffraction peaks shifted toward lower angle, which was due to the substitution of larger Ba^{2+} ions for the smaller Sr^{2+} ions.[22-23] In addition, there was no obvious effect on the structures of the hosts when the activator ions Eu^{2+} were doped into the host. The clear crystal structure provided a good foundation for further study.

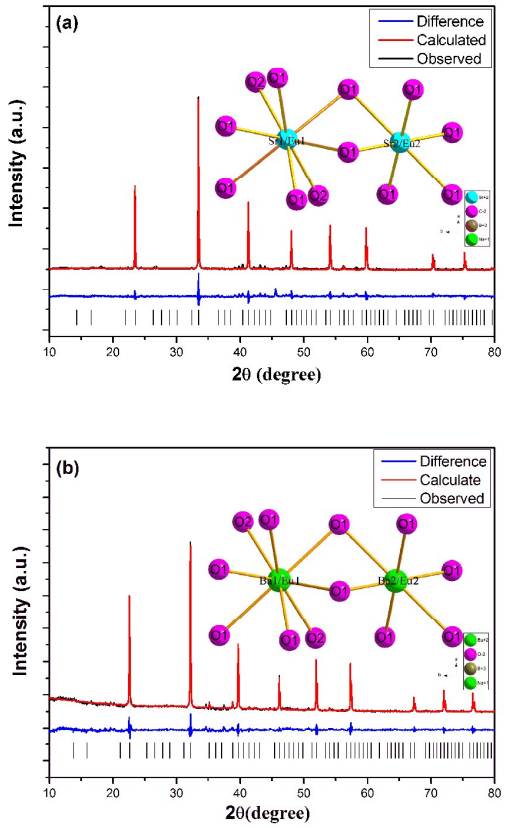

Figure 2 Observed (black), calculated (red), and difference (blue) synchrotron XRD profiles for the Rietveld refinement of (a) $NaSr_{3.98}$ $(BO_3)_3$:$0.02Eu^{2+}$ and (b) $NaBa_{3.98}(BO_3)_3$:$0.02Eu^{2+}$. Bragg reflections are indicated with tick marks.

Figure 2 showed the Rietveld refinement results of $NaSr_{3.98}(BO_3)_3$: $0.02Eu^{2+}$ and $NaBa_{3.98}(BO_3)_3$: $0.02Eu^{2+}$ phosphors, the XRD profiles were indicated as difference (blue), calculated (red) and observed (black), respectively. The single crystal structures data of $NaSr_4(BO_3)_3$ (ICSD # 170862) and $NaBa_4(BO_3)_3$ (ICSD # 170863) were used as the original model to refine the experimental crystal structures. $NaSr_{3.98}(BO_3)_3$: $0.02Eu^{2+}$ and $NaBa_{3.98}(BO_3)_3$: $0.02Eu^{2+}$ crystallized in a cubic unit cell with the same space group *Ia-3d*. In $NaSr_{3.98}(BO_3)_3$: $0.02Eu^{2+}$ host the lattice constants $a = b = c$= 15.0710 (Å) and cell volume=3423.15 (Å^3). In $NaBa_{3.98}(BO_3)_3$: $0.02Eu^{2+}$ host the lattice constants $a = b = c$ = 15.7266 (Å) and cell volume=3889.61 (Å^3). It showed that when the value of doped activator ions y = 0.02, the host of the sample remain a single-phase structure. The detailed refinement results were showed in Table 1.

Table 1 Rietveld refinement and crystal data of $NaSr_{3.98-x}Ba_x(BO_3)_3$: $0.02Eu^{2+}$ phosphors

Compound	x=0	x=3.98
Formula	$NaSr_{3.98}(BO_3)_3$: $0.02Eu^{2+}$	$NaBa_{3.98}(BO_3)_3$: $0.02Eu^{2+}$
Cryst.syst.	Cubic	Cubic
Space group	La-3d(230)	La-3d(230)
Crystal density (g cm^{-3})	6.642	7.534
Unite,Z	16	16
a (Å) = b (Å) = c (Å)	15.0710	15.7266
V ($Å^3$)	3423.15	3889.61
R_{exp} (%)	4.61	3.57
R_{wp} (%)	5.13	4.01
R_p (%)	4.46	3.54
GOF	1.57	1.23

Both the $NaSr_4(BO_3)_3$ and $NaBa_4(BO_3)_3$ hosts have two different coordination environments: Ba^{2+} or Sr^{2+} eight-coordinated with oxygen and six-coordinated with oxygen (see the inset in Figure 2). The ionic radius of Sr^{2+} was 1.18 Å (coordinated number, CN = 6) and 1.26 Å (CN = 8). The ionic radius of Ba^{2+} was 1.35 Å (CN = 6) and 1.42 Å (CN = 8). The ionic radii of Eu^{2+} were 1.17 Å (CN = 6) and 1.25 Å (CN = 8). Because of the similarity in ionic radius, the Sr^{2+} and Ba^{2+} ions sites would be occupied randomly by the Eu^{2+} ions in the $NaSr_4(BO_3)_3$ and $NaBa_4(BO_3)_3$ hosts. which would form eight-coordinated Eu1 and six-coordinated Eu2 sites.[24-25] Meanwhile, when Sr^{2+} or Ba^{2+} ions were replaced by Eu^{2+} ions, two different emission centrers would be obtained by Gaussian fitting in the emission spectra.

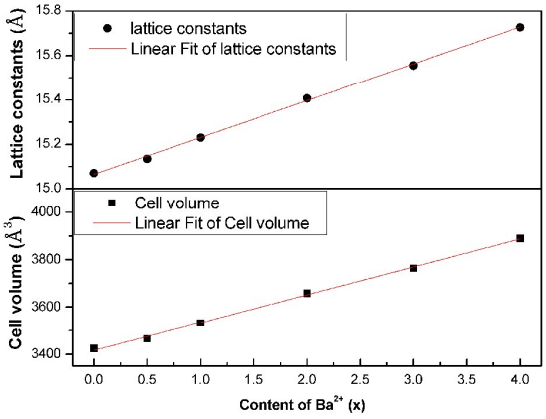

Figure 3 Relationships of lattice constants and cell volume versus the content of Ba^{2+} ions in $NaSr_{4-x}Ba_x(BO_3)_3$ host.

Figure 3 showed the linear relationship of the refined lattice constants and cell volume of the $NaSr_{4-x}Ba_x(BO_3)_3$ host. For the ionic radii of Ba^{2+} ions was bigger than that of Sr^{2+} ions, the lattice constants and cell volume increased gradually with the increase of Ba^{2+} ions concentration. Combining with the analysis of XRD, it was clear that the Sr^{2+} and Ba^{2+} ions substituted each other completely.

3.2 Diffuse reflection spectra

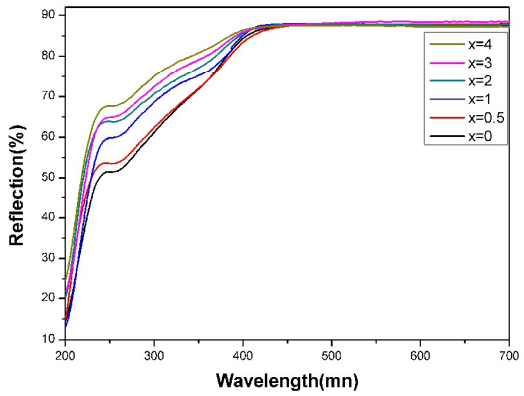

Figure 4 Diffuse reflection spectra of undoped $NaSr_{4-x}Ba_x(BO_3)_3$ samples.

The diffuse reflection spectra of the undoped $NaSr_{4-x}Ba_x(BO_3)_3$ samples were shown in Figure 4. In the visible range (400 -700 nm**)** the sample of $NaSr_{4-x}Ba_x(BO_3)_3$ showed a high reflection. The undoped $NaSr_{4-x}Ba_x(BO_3)_3$ samples showed energy absorption in the 200 - 425 nm range and have a sharp drop between 200 nm and 245 nm. The absorption edge shifted toward short wavelength with the increase of Ba^{2+} ions concentration.

Table 2 Band gap of $NaSr_{4-x}Ba_x(BO_3)_3$,and spectral parameters of $NaSr_{3.98-x}Ba_x(BO_3)_3$: $0.02Eu^{2+}$ phosphors.

Sample x	Band gap (E_v)	Excition maximum (nm)	Emission Maximum (nm)	Stocks shift (cm^{-1})	FWHM (nm)
0	5.86	390	609	9221	134
0.5	5.83	395	585	8222	122
1	5.54	397	570	7645	116
2	5.49	396	562	7459	107
3	5.41	397	550	7007	102
3.98	5.38	397	544	6807	92

The band gap energy (absorption edge) of $NaSr_{4-x}Ba_x(BO_3)_3$ host had been calculated by following equation:[26]

$$[F(R_\infty)hv]^n = A(hv - E_g) \quad (1)$$

where E_g is the value of band gap, A is a proportional constant, hv is the photon energy, for an indirect transition n = 1/2 or for a direct transition n = 2, and the Kubelka-Munk function $F(R_\infty)$ is defined as:[27]

$$F(R) = (1-R)^2 / 2R = K / S \quad (2)$$

Here, S is the scattering coefficient, K is the absorption coefficient and R is the reflection coefficient. From the liner extrapolation of $[F(R_\infty)hv]^2 = 0$, the value of E_g was increased from 5.38 eV to 5.86 eV (see Table 2) with the increasing content of Ba^{2+} ions in the $NaSr_{4-x}Ba_x(BO_3)_3$ phosphor.

3.3 Photoluminescence properties

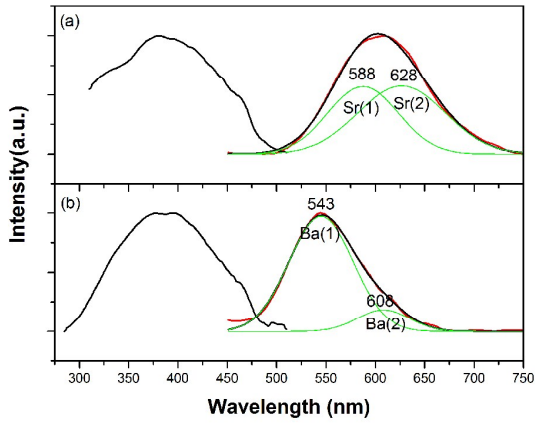

Figure 5 Excitation (left) and emission (right) spectra of (a) $NaSr_{3.98}(BO_3)_3$: $0.02Eu^{2+}$ (λ_{ex}: 390 nm, λ_{em}: 609 nm) and (b) $NaBa_{3.98}(BO_3)_3$: $0.02Eu^{2+}$ (λ_{ex}: 397 nm, λ_{em}: 544 nm) phosphors, fitted curve (red solid line) and deconvoluted Gaussian components (green solid lines).

Figure 5 shows the emission and excitation spectra of (a) $NaSr_{3.98}(BO_3)_3$: $0.02Eu^{2+}$, (b) $NaBa_{3.98}(BO_3)_3$: $0.02Eu^{2+}$, and the deconvoluted Gaussian components. Due to the $4f^7 \rightarrow 4f^6 5d^1$ transition of the Eu^{2+} ions, the excitation peaks show a broad range from 300 nm to 470 nm. As the excitation range of the near ultraviolet LED chip is 380 nm - 420 nm and the blue LED chip is 450-460nm, so they match well with these broad excitation band phosphors. The emission spectra of the $NaSr_{3.98}(BO_3)_3$: $0.02Eu^{2+}$ and $NaBa_{3.98}(BO_3)_3$: $0.02Eu^{2+}$ phosphors show a broad range from 500 nm to 750 nm and 450 nm to 670 nm respectively, which are attributed to the $4f^6 5d^1 \rightarrow 4f^7$ transition of the Eu^{2+} ions. The FWHM (full width at half maximum) of the emission spectra of the $NaSr_{3.98}(BO_3)_3$: $0.02Eu^{2+}$ phosphor is about 134nm, which is wider than other rare earth doped orthoborate phosphors. Although the wide FWHM will decrease the intensity of the emission spectra but it can increase the rendering index which is more important to a white LED. The FWHM of the emission spectra of the $NaBa_{3.98}(BO_3)_3$: $0.02Eu^{2+}$ phosphor is about 92nm, which is similar to other phosphors(see details in Table 2). The emission spectra of the $NaSr_{3.98}(BO_3)_3$: $0.02Eu^{2+}$ and $NaBa_{3.98}(BO_3)_3$: $0.02Eu^{2+}$ phosphors were decomposed into two Gaussian profiles with peaks at 588 nm (17 006 cm^{-1}), 628 nm (15 924 cm^{-1}) (Fig. 5a, solid lines of green), and 543 nm (18 416 cm^{-1}), 608 nm (16 447 cm^{-1}) (Fig. 5b, solid lines of green) respectively, by using the Gaussian deconvolution. The two peaks were caused by two different emission sites, which could be identified as the Eu^{2+} ions occupied the six- and eight-coordinated coordination environments of the Sr^{2+}/Ba^{2+} ions in the host.

Moreover, the local environment of Eu^{2+} ion is a very important factor to its emission position. There is an empirical relation between the local structure and the energetic position of the emission in various compounds. This formula applies equally to $5d$ level positions of Eu^{2+} ions, for the similarity of the Ce^{2+} ion and Eu^{2+} ion in $5d$ levels. The equation is given as follows:[28,29]

$$E = Q \times [1 - (\frac{V}{4})^{\frac{1}{V}} \times 10^{-\frac{n \times E_a \times r}{80}}] \quad (3)$$

where E_a represents the electron affinity of the atoms that form anions, r (Å) is the radius of the host cation replaced by the Eu^{2+} ion, n represents the number of anions in the immediate shell about this ion, V represents the valence of the Eu^{2+} ion, Q represents the position in energy for the lower d-band edge of the Eu^{2+} free ions, and E represents the real position of the d-band edge in energy for the Eu^{2+} ion. There are two Ba^{2+}/Sr^{2+} sites in $NaM_{3.98}(BO_3)_3$: $0.02Eu^{2+}$ (M=Ba, Sr) structure. Most of th e parameters in the equation (3) keep invariable, so that the relationship between observed position of the d-band edge for Eu^{2+} ions and the coordination number n is a proportional relationship. As a result, Eu^{2+} ions center showing emission peak at 543nm and 585nm occupied the eight-coordinated Ba^{2+}/Sr^{2+} site respectively, and the other Eu^{2+} ions center showing 608nm and 628nm was related to the six-coordinated Ba^{2+}/Sr^{2+} ions site, respectively.

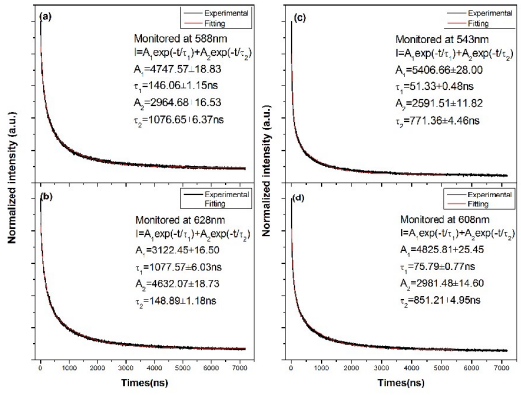

Figure 6 Decay curves of Eu^{2+} emission in $NaSr_{3.98}(BO_3)_3$: .$02Eu^{2+}$ phosphor monitored at (a) 588nm, (b) 628nm, and the $NaBa_{3.98}(BO_3)_3$: $0.02Eu^{2+}$ phosphor monitored at (c) 534nm, (d) 608nm.

Figure 6 demonstrated the fluorescence decay curves of $NaSr_{3.98}(BO_3)_3$: $0.02Eu^{2+}$ and $NaBa_{3.98}(BO_3)_3$: $0.02Eu^{2+}$ phosphors in different coordination environments, eight-coordinated and six-coordinated respectively. The following formula can be used to calculate the decay times:

$$I = A_1 \exp(-t / \tau_1) + A_2 \exp(-t / \tau_2) \quad (4)$$

Where τ_1 and τ_2 are exponential components of the decay times, A_1 and A_2 are constants, t is time, and I is phosphorescence

intensity. The following formula can calculate the average decay times (τ*):[30]

$$<\tau^*>=(A_1\tau_1^2+A_2\tau_2^2)/(A_1\tau_1+A_2\tau_2) \quad (5)$$

Through quote the relevant experimental data, the value of the average decay times (τ*) are 910.56 ns (monitored at 588 nm) and 927.31 ns (monitored at 628nm) for $NaSr_{3.98}(BO_3)_3$: $0.02Eu^{2+}$ phosphor, and 683.58ns (monitored at 543 nm) and 753.53 ns (monitored at 608nm) for $NaBa_{3.98}(BO_3)_3$: $0.02Eu^{2+}$. It is again prove that the Eu^{2+} ions occupied two different Sr^{2+} and Ba^{2+} ions positions by the results above.

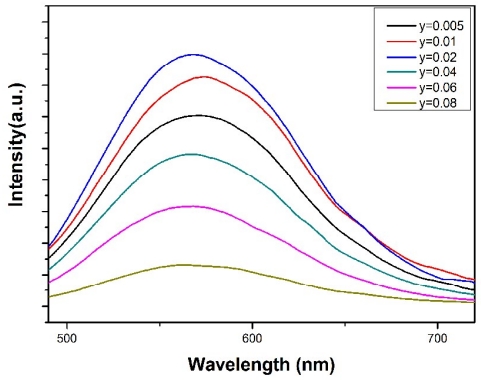

Figure 7 Emission spectra of $NaSr_{3-y}Ba(BO_3)_3$:yEu^{2+} sample under 395nm UV light excitation.

Figure 7 represents the emission intensity of $NaSr_{3-y}Ba(BO_3)_3$: yEu^{2+} phosphor with the various Eu^{2+} concentration. With the increase of the Eu^{2+} ions content, the emission and excitation intensity enhanced gradually. When the Eu^{2+} concentration at the value of y=0.02, the emission intensity reaches a maximum value. The concentration quenching emerged when the Eu^{2+} content over 0.02 and the emission intensity comes into a decrease tendency. The multipole-multipole interaction, radiation reabsorption or exchange interaction are three different ways may cause the non-radiative energy transfer between different Eu^{2+} ions.[31,32] A formula proposed by Blasse can be used to calculate the critical distance for energy transfer in $NaSr_{3-y}Ba(BO_3)_3$:yEu^{2+} for Eu^{2+} ion.[33]

$$R_c \approx 2\left(\frac{3V}{4\pi\chi_c N}\right)^{\frac{1}{3}} \quad (6)$$

where N is the number of available sites (cations) that can be occupied by activator ion, χ_c is the critical concentration of the Eu^{2+} ion, V is the volume of the unit cell, and R_c is the critical distance at the critical concentration between the nearest Eu^{2+} ions. Herein V=3535.1 Å^3, N=16, and χ_c=0.02 in the $NaSr_{3-y}Ba(BO_3)_3$: yEu^{2+}. The calculated critical distance R_c is 27.63 Å. According to Dexter's theory, the electric multipolar interactions can cause the non-radiative energy transfer between Eu^{2+} ions.[34] When the energy transfer occurs between the same active ions, the intensity of the multipolar interaction can be determined by the emission intensity. The following equation can express the emission intensity (I) per activator ion in the host:[35,36]

$$\frac{1}{\chi}=\frac{k}{1+\beta(\chi)^{\frac{\theta}{3}}} \quad (7)$$

Where under the same excitation condition in the same host crystal k and β are constants, χ is the critical concentration of the activator ions, according to the previous report, θ=3 is for the energy transfer between the nearest-neighbor ions, while θ=10 is for quadrupole-quadrupole (q-q) interaction, θ=8 is for dipole-quadrupole (d-q) interaction, and θ=6 is for dipole-dipole (d-d) interaction. Figure 8 presents linear relationship between log(I/$y$$Eu^{2+}$) and log($y$$Eu^{2+}$), and the value of slope liner is equivalent to -θ/3. Its calculated slope is -1.74, so the value of θ is 5.22, which is close to 6. The result illustrated that the concentration quenching mechanism between Eu^{2+} ions in the $NaSr_{3-y}Ba(BO_3)_3$: yEu^{2+} host was confirmed to be dipole-dipole interaction.

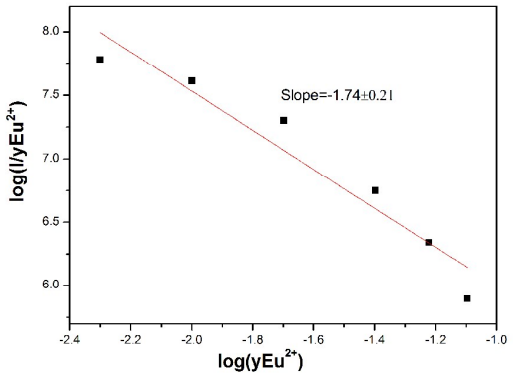

Figure 8 Relationships of log(I/$y$$Eu^{2+}$) versus log($y$$Eu^{2+}$) in $NaSr_{3-y}Ba(BO_3)_3$: yEu^{2+} phosphor.

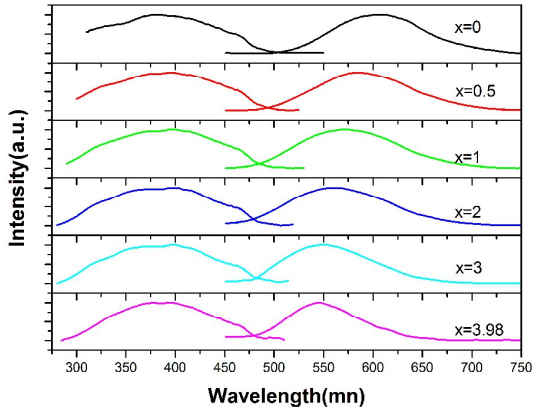

Figure 9 Emission and excitation spectra of $NaSr_{3.98-x}Ba_x(BO_3)_3$: $0.02Eu^{2+}$

The excitation and emission spectra of $NaSr_{3.98-x}Ba_x(BO_3)_3$: $0.02Eu^{2+}$ are shown in Figure 9. With the increase of Sr^{2+} substituted by Ba^{2+} ions, an obvious blue-shift of the emission spectra could be observed, which changed from 609 nm (x=0) to 544 nm (x=3.98) (see details in Table. 2). There is no distinct change in the excitation spectra.

The following two factors should to be considered for the blue-shift of the emission spectra. The Nephelauxetic effect can cause a higher $4f^6 5d^1$ band position.[37,38] The electronegativity of Sr (0.95) is higher than that of Ba (0.89).[39] With the increase of the concentration of Ba^{2+} ions, the difference of electronegativity between anion and cation increased, and hence the covalency decreased in the host. That is, the blue-shift of the emission of Eu^{2+} can be explained by covalent nature decrease depend on the Nephelauxetic effect.

Table 3 Average distance (R_{av}) between the activator (Sr^{2+}/Ba^{2+}) and the neighboring anions (O^{2-}) in $NaSr_{4-x}Ba_x(BO_3)_3$ samples

Compound	x=0	x=0.5	x=1	x=2	x=3	x=3.98
Average distance (R_{av})(Å)	2.6124	2.6634	2.6893	2.7130	2.7478	2.7727

The crystal filed splitting is another important factor to the blue-shift phononemon.[40] The polyhedron have a great influence on the crystal field splitting which can be denoted by the ε_{cfs} value.[41,42] A great blue-shift may due to a small ε_{cfs} value. Dorenbos P. concluded that Eu^{2+} in a larger coordinating polyhedron would have a smaller crystal field splitting of 5d levels.[43-46] The ε_{cfs} value has an empirical relationship with the average distance (R_{av}):

$$\varepsilon_{cfs} = \beta_{poly}^{Q} R_{av}^{-2} \quad (8)$$

where Q is 2 for Eu^{2+}, R_{av} is average distance between the Eu^{2+} ion and the neighbor anions, and β_{poly} is a constant which its value depends on the type of the coordinating polyhedron. β_{poly} values are in the ratio 0.42, 0.79, 0.89, and 1, for tricapped trigonal prismatic coordination, dodecahedral, cubic, and octahedral, respectively. [47] With the increase of the average distance (R_{av}) (see Table 3), ε_{cfs} is likely to decrease, which causes a blue-shift of the emission of $NaSr_{3.98-x}Ba_x(BO_3)_3$: $0.02Eu^{2+}$ phosphor.

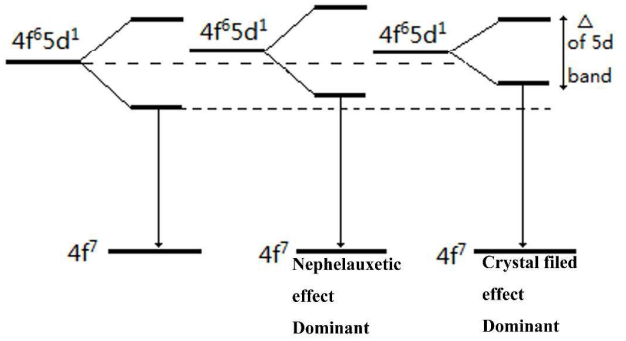

Figure 10 Schematic diagram of energy band change of Eu^{2+} in the $NaSr_{3.98-x-y}Ba_x(BO_3)_3$: yEu^{2+} host.(Δ represents the crystal filed splitting of the 5d level of the Eu^{2+} ions.)

The schematic diagram for the effects of crystal filed splitting and covalency (Nephelauxetic effect) on the energy level of Eu^{2+} ions were shown in Figure 10. In this system, the crystal field splitting and Nephelauxetic effect have common influence on the 5d level when the Sr^{2+} was replaced by Ba^{2+} site.[48] As the concentration of Ba^{2+} ions increased, the covalency decreased and the position of $4f^6 5d^1$ level of Eu^{2+} increased in the host. On other hand, the 5d lowest level increases due to crystal filed splitting decrease. Therefore, the emission band change is due to the influence of the crystal filed splitting and covalency.

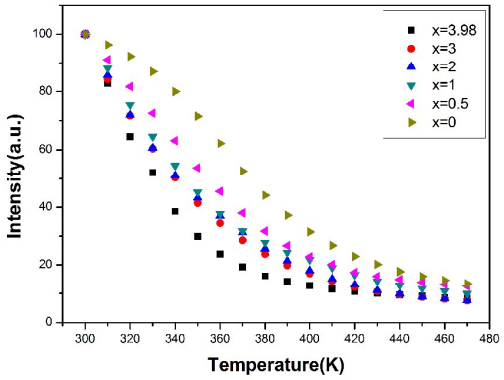

Figure 11 Relationships for the emission intensity of $NaSr_{3.98-x}Ba_x(BO_3)_3$: $0.02Eu^{2+}$ phosphors and operating temperature (**K**)

Thermal stability is an important factor for luminescent materials, due to the quenching effect of temperature, the emission intensity of most of the luminescent materials decreases with the increase of temperature.[49,50] Figure 11 shows the relationship between temperature and emission intensity of the $NaSr_{3.98-x}Ba_x(BO_3)_3$: $0.02Eu^{2+}$ phosphors. The emission intensity was collected, processed and monitored at 400nm under a continuously change of operating temperature (**K**) to analysze the thermal stability of the phosphors. With the increasing of the Ba^{2+} contents in $NaSr_{3.98-x}Ba_x(BO_3)_3$: $0.02Eu^{2+}$ host, the thermal stability of the phosphors decreased gradually.

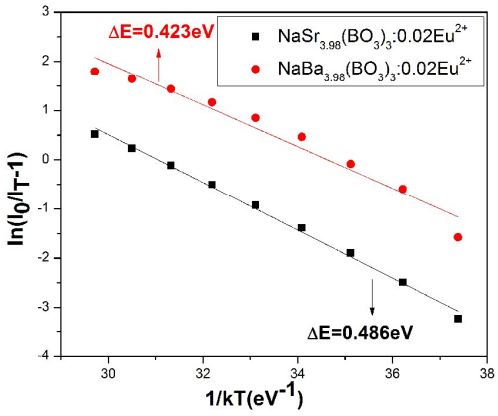

Figure 12 Plots of $\ln[(I_0/I_T)-1]$ and 1/kT for $NaSr_{3.98}(BO_3)_3$: $0.02Eu^{2+}$ and $NaBa_{3.98}(BO_3)_3$: $0.02Eu^{2+}$.

Furthermore, the activation energy ΔE (the energy that a electron needed to raise from the relaxed excited level to the host lattice conduction band) of the activator ion, can be obtained by following formula:[51-56]

$$I_T = I_0[1 + c\exp(-\frac{\Delta E}{kT})]^{-1} \quad (9)$$

here k represents the Boltzmann constant (8.629×10^{-5} eV K^{-1}), ΔE represents the activation energy, c is a constant, I_T represents the intensity of the emission spectrum at the temperature of T, and I_0 represent the initial emission intensity. The relationship between $1/k$ and $T\ln[(I_0/I_T)-1]$ for $NaSr_{3.98}(BO_3)_3$: $0.02Eu^{2+}$ and $NaBa_{3.98}(BO_3)_3$: $0.02Eu^{2+}$ are shown in Figure 12. According to equation (9), the value of the ΔE is calculated to be 0.486 eV for $NaSr_{3.98}(BO_3)_3$: $0.02Eu^{2+}$ and 0.423 eV for $NaBa_{3.98}(BO_3)_3$: $0.02Eu^{2+}$. The calculated value ΔE of $NaSr_{3.98}(BO_3)_3$: $0.02Eu^{2+}$ phosphor is bigger than that of $NaBa_{3.98}(BO_3)_3$: $0.02Eu^{2+}$ phosphor. Therefore, the thermal stability of $NaSr_{3.98}(BO_3)_3$: $0.02Eu^{2+}$ phosphor is better than $NaBa_{3.98}(BO_3)_3$: $0.02Eu^{2+}$ phosphor.

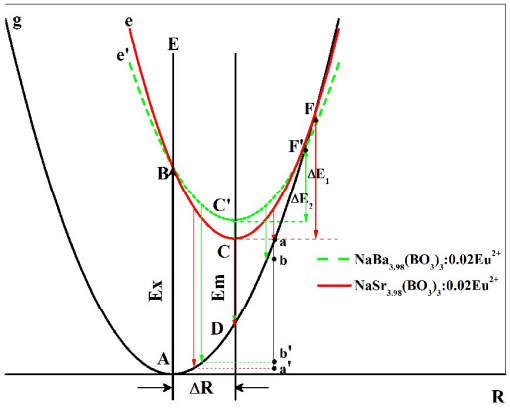

Figure 13 Configuration coordinate diagram of $NaSr_{3.98-x}Ba_x(BO_3)_3$: $0.02Eu^{2+}$ phosphors.

Figure 13 shows the configuration coordinate diagram of $NaSr_{3.98}(BO_3)_3$: $0.02Eu^{2+}$ and $NaBa_{3.98}(BO_3)_3$: $0.02Eu^{2+}$ phosphors. The energy **E** is plotted versus the metal-ligand **R**, and **R** is the structural parameter which changes during the vibration. The curve of **g** represent the ground state, the curves of **e** and **e′** represent the excited state of the Eu^{2+} ions emission center in $NaSr_{3.98}(BO_3)_3$: $0.02Eu^{2+}$ and $NaBa_{3.98}(BO_3)_3$: $0.02Eu^{2+}$, respectively. The electronic transitions can be considered as four steps.[57] Firstly, an electron is promoted from the ground state **A** to the excited state **B**. Secondly, the electron relaxes from the excited state **B** to the bottom of the excited state **C/C′**. It is a non-radiative process. Thirdly, the electron relaxes from the bottom of the excited state **C/C′** to the ground state **D** by photo emission. At the last, the electron relaxes from ground state position **D** to the lowest ground state position **A**.

When Sr^{2+} site was substituted by Ba^{2+}, the 5*d* levels crystal field splitting of Eu^{2+} ions is decreased, the excited state of the Eu^{2+} emission center changed from curve **e** to **e′**, and the bottom of the excited state **C** up to the **C′**. As a result, the emission peaks shift toward shorter wavelength and the Stokes shift decreased (as shown in Table 2). Furthermore, the **a-a′** and **b-b′** represent the FWHM of emission spectra. The distance between **a-a′** is larger than **b-b′**. It means that the FWHM of emission spectra are narrowed when Sr^{2+} ions were substituted by Ba^{2+} ions. In other hand, the cross point **B** did not change evidently when Sr^{2+} was substituted by Ba^{2+} ions. It can be certified by the hardly change of excitation peaks of $NaSr_{3.98-x}Ba_x(BO_3)_3$: $0.02Eu^{2+}$ (see Table 2). However, when the temperature increase, electron–phonon coupling can cause the thermal activation and the energy reaches the crossing point (**F/F′**) between the ground and excited states.[58,59] In this situation, non-radiative relaxation occurs by heat dissipation and quench the luminescence.[60] With the increase of Ba^{2+} ions content in the $NaSr_{3.98-x}Ba_x(BO_3)_3$: $0.02Eu^{2+}$ phosphors, the thermal activation energy decreased ($\Delta E_2 < \Delta E_1$) which can verify the result of the ΔE that concluded from Figure 11 and Figure 12.

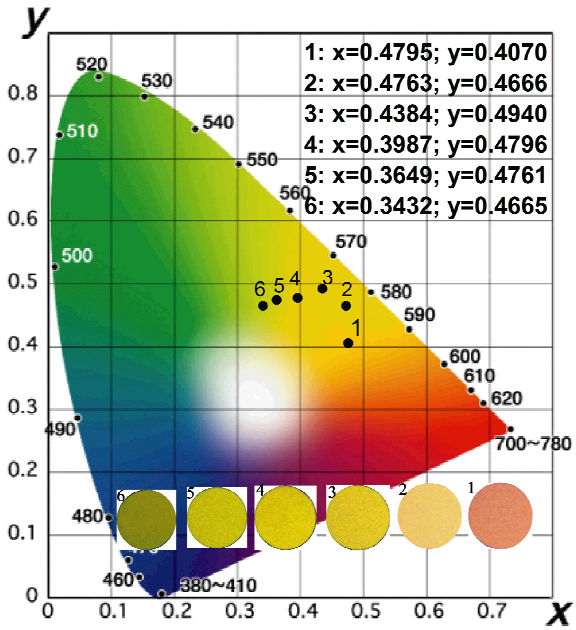

Figure 14 Variation in CIE chromaticity coordinates as a function of x in $NaSr_{3.98-x}Ba_x(BO_3)_3$: $0.02Eu^{2+}$. The inset shows the luminescence of $NaSr_{3.98-x}Ba_x(BO_3)_3$: $0.02Eu^{2+}$ photos taken under 365nm excitation.(x=0, 0.5, 1, 2, 3 and 3.98).

Figure 14 shows the CIE chromaticity coordinates for the $NaSr_{3.98-x}Ba_x(BO_3)_3$: $0.02Eu^{2+}$ phosphors with different value of *x*. The inset shows the $NaSr_{3.98-x}Ba_x(BO_3)_3$: $0.02Eu^{2+}$ photos taken under 365nm excitation. The corresponding chormaticity coordinates(*x*, *y*) is turning from (0.4795, 0.4070) to (0.3432, 0.4665). The color hue can turn continuously from orange (544 nm) to yellow-green (609 nm). Therefore, the $NaSr_{(4-x-y)}Ba_x(BO_3)_3$: yEu^{2+} phosphor has a great property of situation tunable emission, and it has a great potential that be applied as a color conversion material for light emitting diodes.

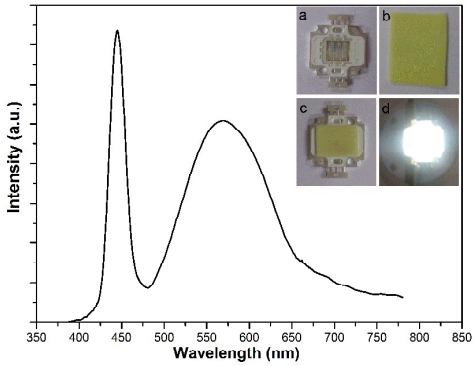

Figure 15 Electroluminescence spectrum of the white LED consisting of the $NaSr_{2.98}Ba(BO_3)_3$: $0.02Eu^{2+}$ phosphor and a 450 nm blue LED chip under a applied current of 100 mA. The inset shows the photograph of (a) 450 nm blue LED chip, (b) epoxy resin mixed with phosphor film (c) prepared LED , (d) LED in operation, respectively.

Figure 15 shows the electroluminescence spectrum of the white LED consisting of the $NaSr_{2.98}Ba(BO_3)_3$: $0.02Eu^{2+}$ phosphor and a 450 nm blue LED chip under a applied current of 100 mA. The inset shows the photograph of (a) 450 nm blue LED chip, (b) epoxy resin mixed with phosphor film (c) prepared LED, (d) LED in operation, respectively. The white LED had CIE color coordinates of (0.3563, 0.3576) with a color-rendering index of 85.3 around the correlated color temperature of 5083 K. This result confirms that the $NaSr_{3.98-x}Ba_x(BO_3)_3$: $0.02Eu^{2+}$ have potential for application in white LED.

4. Conclusions

In summary, the continuously tunable-emission Eu^{2+} doped $NaSr_{4-x}Ba_x(BO_3)_3$ phosphor have been synthesized successfully by a conventional high temperature solid-state reaction in the reductive atmosphere with a relatively lower temperature. The crystal structure and luminescence properties were investigated systematically. With the increase of Ba^{2+} ions in the $NaSr_{4-x}Ba_x(BO_3)_3$ host, the lattice constants and cell volume increased gradually, while the crystal structure remained cubic unit cell which can be confirmed by the X-ray diffraction patterns and Rietveld refinement. From the analytical data of the crystal structure, the band structure and the emission spectra, the continuously tunable emission from longer to shorter wavelength have been proved to be the combined effect of the crystal filed splitting and Nephelauxetic effect. The concentration quenching of Eu^{2+} ions emission in $NaSr_{3-y}Ba(BO_3)_3$: yEu^{2+} host lattice is due to the electric dipole-dipole interaction. Due to the decrease of the $\Delta\mathbf{E}$, the thermal stability of $NaSr_{3-y}Ba(BO_3)_3$: yEu^{2+} become lower with the increase of Ba^{2+} ions content. The emission colors of the obtained phosphors can be continuously tuned from orange-red (0.4795, 0.4070) to yellow-green (0.3432, 0.4665) by adjusting the doping substitution content of Ba^{2+} ions. The packed white LED had CIE color coordinates of (0.3563, 0.3576). This results demonstrate that the $NaSr_{(4-x-y)}Ba_x(BO_3)_3$: yEu^{2+} phosphor has a great potential that be applied as a color conversion material for light emitting diodes.

Acknowledgements

This research is supported by Zhejiang Provincial Natural Science Foundation of China under Grant No. LR14A040002 and LQ13E020003, the Project of the National Nature Science Foundation of China under Grant No 51402077, 51272243, 61370049 and 61405185. The project of Zhejiang province College Students' Science and Technology Innovation (2014R409035)

References

1 E. Schubert and J. Kim, *Science*, 2005, **308**, 1274-1278.
2 Y. Narukawa, J. Narita, T. Sakamoto, T.Yamada, H. Narimatsu, M. Sano and T. Mukai, *Phys. Status. Solidi. A*, 2007, **204**, 2087-2093.
3 W. B. Im, Y. I. Kim, N. N. Fellows, H. Masui and G. A. Hirata. *Appl. Phys. Lett.*, 2008, **93**, 091905-091905-3.
4 T. Nishida, T. Ban and N. Kobayashi, *Appl. Phys. Lett.*, 2003, **82**, 3817-3819.

5 J. S. Kim, P. E. Jeon, J. C. Choi, H. L. Park, S. I. Mho and G. C. Kim, *Appl. Phys. Lett.*, 2009, **84**, 2931-2933.
6 G. Blasse and A. Bril, *Appl. Phys. Lett.*, 1997, **11**, 53-55.
7 G. Blasse and A. Bril, *J. Chem. Phys.*, 1997, **47**, 5139-5145.
8 K. A. Denault, A. A. Mikhailovsky, S. Brinkley, S. P. DenBaars and R. Seshadri, *J. Mater. Chem. M*, 2013, **1**, 1461-1466.
9 A. Setlur, V. E. Radkov, S. C. Henderson, J. Her, M. A. Srivastava, N. Karkada, M. Kishore and N. Kumar, et al. *Chem. Mater.*, 2010, **22**, 4076-4082.
10 W. Im, S. Brinkley, J. Hu, A. Mikhailovsky, S. DenBaars and R. Seshadri, *Chem. Mater.*, 2010, **22**, 2842-2849.
11 Y. Wu, D. Wang, T. Chen, C. Lee, K. Chen and H. Kuo, *ACS Appl. Mater. Interfaces*, 2011, **3**, 3195-3199.
12 H. Yu, D. Deng, D. Zhou, W. Yuan, Q. Zhao, Y. Hua, S. Zhao, L. Huang and S. Xu, *J. Mater. Chem. C*, 2013, **1**, 5577-5582.
13 X. Zhou, X.Yang, Y. Wang, X. Zhao, L. Li and Q. Li, *J. Alloy. Comp.*, 2014, **608**, 25-29.
14 T. R. N. Kutty, *Mater. Res. Bull.*,1990, **25**, 343-348.
15 S. Jian, L. Zhi, S. Guang, and S. De, *Rsc Advances.*, 2013, **3**, 18395-18405.
16 Z. Xing, J. Xiao, L. Hu, L. Zun, M. Xiao, M. Fan, Z. Jian and T. Cheng, *Rsc Advances*, 2015, **5**, 40864-40871..
17 H. Liang, G. Zhang, P. Dorenbos and Q. Su, *J. Lumin.*, 2001, **131**, 194-198.
18 X. Zhang, X. Zhang and H. J. Seo, *Physica B*, 2011, **406**, 77-79.
19 O. Aloui-Lebbou, C. Goutaudier, S. Kubota, C. Dujardin, M.T. Cohen-Adad, C. Pédrini, P. Florian and D. Massiot, *Opt. Mater.*, 2001, **16**, 77-86.
20 X. Zhang, L. Zhou and M. Gong, *J. Biolumin. Chemilumin.*, 2014, **29**, 104-108.
21 G. Li, Y. Wang, W. Zeng, S. Han, W. Chen, Y. Li and H. Li, *Opt. Mater.*, 2014, **36**, 1808-1813.
22 L. Wu, X. L. Chen, H. Li, M. He, Y. P. Xu and X. Z. Li, *Inorg. Chem.*, 2005, **44**, 6409-6414.
23 K. A. Denault, J. Brgoch, M. W. Gaultois, A. Mikhailovsky, R.Petry, H. Winkler, S. P. DenBaars and R. Seshadri, *Chem. Mater.*, 2014, **26**, 2275-2282.
24 G. Li, C. C. Lin, W. T. Chen, M. S. Molokeev, V. V. Atuchin, C. Y. Chiang, W. Zhou and C. W. Wang, et al. *Chem. Mater.*, 2014, **26**, 2991-3001.
25 S. Miao, Z. Xia, M. S. Molokeev, M. Chen, J. Zhang and Q. Liu, *J. Mater. Chem. C*, 2015, **3**, 4616-4622.
26 Z. Jiang, Y. Wang and L. Wang, *J. Electrochem. Soc.*, 2009, **157**, 155-158.
27 A. E. Morales, E. S. Mora and U. Pal, *Rev. Mex. Fis.*, 2007, **53**, 18-22.
28 M. Shang, G. Li, D. Geng, D. Yang, X. Kang, Y. Zhang, H. Lian and J. Lin, *J. Phys. Chem. C*, 2012, **116**, 10222-10231.
29 L. V. Uitert, *J. Lumin.*, 1984, **29**, 1-9.
30 N. Ruelle, M. Pham-Thi and C. Fouassier, *JJAP*, 1992, **31**, 2786-2790.
31 H. Yu, D. Deng, D. Zhou, Y. Wei, Q. Zhao and Y. Hua, *J. Mater. Chem. C*, 2013, **1**, 5577-5582.
32 D. Deng, H. Yu, Y. Li, Y. Hua, G. Jia and S. Zhao, *J. Mater. Chem. C*, 2013, **1**, 3194-3199.
33 G. Blasse, *Phys. Lett. A*, 1968, **28**, 444-445.
34 D. L. Dexter, *J. Chem. Phys.*, 1953, **21**, 836-850.
35 L. G. V. Uitert, *J. Electrochem. Soc.*, 1967, **114**, 1048-1053.
36 L. Zhang, J. Zhang, X. Zhang, Z. Hao, H. Zhao and Y. Luo, *ACS Appl. Mater. Inter.*, 2013, **5**, 12839-128464.
37 J. A. Duffy and M. D. Ingram, *Inorg. Chim. Acta*, 1973, **7**, 594-596.
38 R. Reisfeld and L. Boehm, *J. Non-Cryst. Solids.*,1975, **17**, 209-214.
39 L. Pauling, *Nature*, 1960, **145**, 644-645.
40 J. K. Park, C. H. Kim, S. H. Park, H. D. Park and S. Y. Choi, *Appl. Phys. Lett.*, 2004, **84**, 1647-1649.
41 J. Zhang, W. Zhang, Y. Hea, W. Zhou, L.Yu, S. Lian, Z. Li and M. Gong, *Ceram. Int.*, 2014, **40**, 9831-9834.
42 Y. He, J. Zhang, W. Zhou, J. Han, Z. Qiu, L. Yu, C. Rong and S. Lian, *J. Am. Chem. Soc.*, 2014, **97**, 1517-1522.
43 P. Dorenbos, *Phys. Rev. B*, 2000, **62**, 15640-15649.
44 P. Dorenbos, *Phys. Rev. B*, 2000, **62**, 15650-15659.
45 P. Dorenbos, *Phys. Rev. B*, 2001, **64**, 125-117.
46 P. Dorenbos, *J. Phys. Condens. Mat*, 2003, **15**, 4797-4807.
47 P. Dorenbos, *J. Lumin.*, 2003, **105**, 117-119.
48 H. S. Jang, Y. H. Won, S. Vaidyanathan, K. H. Dong and Y. J. Duk, *J. Electrochem. Soc.*, 2009, **156**, J138-J142.
49 K. A. Denault, J. Brgoch, M. W. Gaultois, A. Mikhailovsky, R. Petry, H. Winkler, S. P. DenBaars and R. Seshadri, *Chem. Mater.*, 2014, **26**, 2275-2282.
50 Y. Huang, J. Gan and H. J.Seo, *J. Am. Chem. Soc.*, 2011, **94**, 1143-1148.
51 Y. Huang, *Opt. Express*, 2011, **19**, 6311-6319.
52 W. Liu, C. Yeh, C. Huang, C. C. Lin, Y. Chiu, Y. Yeh and R. Liu, *J. Mater. Chem.*, 2011, **21**, 3740-3744.
53 Q. Zhang, *Prog. Chem.*, 2011, **3** 2172-2195.
54 D. Geng, M. Shang, Y. Zhang, Z. Cheng and J. Lin, *Eur. J. Inorg. Chem.*, 2013, **2013**, 2947-2953.
55 X. Mi, J. Sun, P. Zhou, P. Zhou, H. Zhou, D. Song and K. Li, *J. Mater. Chem. C*, 2015, **3**, 4471-4481.
56 B. L. Abrams, L. Williams, J. S. Bang and P. H. Holloway, *J. Appl. Phys.*, 2005, **97**, 033521-1-033521-4
57 Y. Hua, H. Ma, D. Deng, S. Zhao, L. Huang, H. Wang and S. Xu, *J. Lumin.*, 2014, **148**, 39-43.
58 G. Li, C. C. Lin, W. T. Chen, M. S. Molokeev, V. V. Atuchin, C. Y. Chiang, W. Zhou and C. W. Wang, et al. *Chem. Mater.*, 2014, **26**, 2991–3001.
59 P. Dorenbos, *J. Phys. Condens. Mat.*, 2005, **17**, 8103-8111.
60 Y. Zhang, X. Li, K. Li, H. Lian, M. Shang and J. Lin, *J. Mater. Chem. C*, 2015, **3**, 3294-3303.